BRITISH JOURNAL OF HOSPITAL MEDICINE

ARTICLE

Can dynamic contrast-enhanced MR imaging based on radiomics improve the diagnostic efficiency of clinically significant prostate cancer?

Yan Wu[1]

Jiaming Tian[2]

Feng Ma[1]

Chipeng Wang[3]

Author details can be found at the end of this article

Correspondence to:
Chipeng Wang
(wangchipeng@126.com)

Abstract

Aims/Background Prostate cancer stands out as one of the most prevalent malignant tumours among males. The non-invasive identification of clinically significant prostate cancer via magnetic resonance imaging plays a critical role in circumventing unnecessary biopsies and determining suitable treatment strategies for patients. Our study aimed to evaluate the potential improvement in predictive accuracy for clinically significant prostate cancer by incorporating perfusion data obtained from dynamic contrast-enhanced magnetic resonance imaging acquisition protocols into multiparametric magnetic resonance imaging parameters.

Methods Radiomics extracted from perfusion parameters (K^{trans}, K_{ep}, V_e) of dynamic contrast-enhanced magnetic resonance imaging were analysed in patients suspected of prostate cancer who underwent 3T multiparametric magnetic resonance imaging between January 2017 and June 2023 in this retrospective study. The pathological findings obtained from biopsy or therapy were categorised into groups based on the Gleason sum score as either clinically significant prostate cancer (Gleason sum score > 7) or non-clinically significant prostate cancer (Gleason sum score ≤ 6). Diagnostic models were constructed using logistic regression analysis, incorporating prostate imaging reporting and data system V2.1 scores and clinical data, with or without radiomics extracted from dynamic contrast-enhanced. The area under curve (AUC) values were compared using the DeLong test.

Results Overall, 214 men (clinically significant prostate cancer [n=78] and non-clinically significant prostate cancer [n=136]) were included. The clinical-prostate imaging reporting and data system model demonstrated an AUC of 0.89 (95% confidence interval: 0.84–0.95) in the training cohort and 0.91 (95% confidence interval: 0.84–0.98) in the test cohort. For the clinical-prostate imaging reporting and data system-radscore model, the AUC values were 0.97 (95% confidence interval: 0.95–0.99) for K^{trans}, 0.98 (95% confidence interval: 0.96–1.00) for V_e, and 0.96 (95% confidence interval: 0.93–0.98) for K_{ep} in the training cohort, and 0.97 (95% confidence interval: 0.94–1.00) for K^{trans}, 0.95 (95% confidence interval: 0.91–1.00) for V_e, and 0.97 (95% confidence interval: 0.94–1.00) for K_{ep} in the test cohort. Radiomics based on perfusion parameters exhibited good diagnostic performance in predicting clinically significant prostate cancer. The clinical-prostate imaging reporting and data system-radscore model demonstrated superior diagnostic capability compared to perfusion-based radiomics or clinical-prostate imaging reporting and data system models alone.

Conclusion The application of radiomics, which involves extracting perfusion parameters from dynamic contrast-enhanced imaging, has the potential to enhance diagnostic accuracy for clinically significant prostate cancer.

Key words: Dynamic contrast-enhanced; Magnetic resonance imaging; Perfusion; Prostate cancer; Radiomics

Submitted: 20 March 2024; Revised: 19 April 2024; Accepted: 05 May 2024

How to cite this article:
Wu Y, Tian J, Ma F, Wang C. Can dynamic contrast-enhanced MR imaging based on radiomics improve the diagnostic efficiency of clinically significant prostate cancer? Br J Hosp Med. 2024. https://doi.org/10.12968/hmed.2024.0131

Introduction

Prostate cancer (PCa) ranks as the second most prevalent cause of cancer-related mortality among men (Siegel et al, 2015). Non-clinically significant prostate cancer (non-csPCa) demonstrates a low incidence of progression and offers potential for cure. Accurately identifying clinically significant lesions is essential for selecting suitable treatment modalities and reducing the risks of overtreatment or ineffective outcomes (Ahmed et al, 2012).

Multiparametric magnetic resonance imaging (mpMRI) of the prostate has continuously advanced in diagnosing clinically significant prostate cancer (csPCa) (Stavrinides et al, 2020), incorporating diffusion-weighted, T2-weighted, and dynamic contrast-enhanced (DCE) parameters. A contentious debate has arisen regarding whether biparametric magnetic resonance imaging (bpMRI), excluding the DCE sequence to reduce image capture time and avoid intravenous contrast agent injection, can substitute for mpMRI due to reported promising diagnostic efficacy in csPCa (Wei et al, 2018; Cindil et al, 2019; Bass et al, 2020). The utility of DCE in diagnosing csPCa remains controversial (Kuhl et al, 2017; Boesen et al, 2018; Bass et al, 2020), with recent studies revealing its value when Diffusion Weighted Imaging (DWI) and/or T2 Weighted Imaging (T2WI) are insufficient (Belue et al, 2022). Further research is necessary to explore the advantages of DCE before endorsing the use of bpMRI.

Previous studies have investigated the diagnostic efficacy of DCE and its quantitative parameters in PCa (Bosaily et al, 2020; Winkel et al, 2020; Zhao et al, 2021; Tavakoli et al, 2023). Radiomics, utilising high-throughput texture data, has long been a focus in tumour prediction research. However, no prior studies have investigated combining quantitative perfusion parameters from DCE with radiomics. We aimed to explore the potential of radiomics derived from quantitative perfusion parameters of DCE-MRI in providing supplementary diagnostic value for identifying csPCa in this study.

Methods

Patients

This retrospective study received approval from the Institutional Review Boards of the Central Hospital of Wuhan (Ethics number: WHZXKYL2024-042). The study protocol complied with the Declaration of Helsinki, and informed consent was obtained from all participants.

The study enrolled 214 patients consecutively diagnosed with biopsy pathology or who underwent surgery and received magnetic resonance imaging (MRI) examinations between January 2017 and June 2023. The inclusion criteria were defined as follows: (1) men suspected of having PCa and undergoing MRI; (2) patients confirmed histologically by biopsy or surgery; (3) the interval between MRI capture and pathological examination was less than 4 weeks. Exclusion criteria included: (1) prior therapy history; (2) absence of visible lesions in magnetic resonance (MR) imaging; (3) significant imaging artefacts in MR imaging; (4) T4 stage patients on MR showing lymph node metastasis or extracapsular invasion. Baseline clinical features, including prostate specific antigen (PSA) levels, were obtained from medical records. The study design is illustrated in **Figures 1,2** and is depicted in a flow diagram.

Pathology

All patients underwent histopathological confirmation by a genitourinary pathologist with over 5 years of experience in genitourinary pathology via surgical specimens or transrectal ultrasound-guided 12-core systematic biopsy. Clinically significant prostate cancer was characterised by a Gleason score ≥7, whereas non-significant prostate lesions encompassed GS <7, including clinically insignificant prostate cancer (ciPCa) and benign lesions.

Clinical data

We gathered clinical data, encompassing age, prostate volume (PV), serum PSA (total PSA and free PSA), PSAD (prostate specific antigen density), and prostate biopsy pathology from the selected patients. Prostate volume (PV) was computed as width × length × height × 0.52 based on T2-weighted images. PSAD was derived by dividing total PSA by PV.

Magnetic resonance imaging examination

All enrolled patients underwent imaging using a 3.0 T MRI scanner (Philips-Ingenia, Philips Healthcare, Eindhoven, The Netherlands) equipped with a 32-channel pelvic coil. The scan

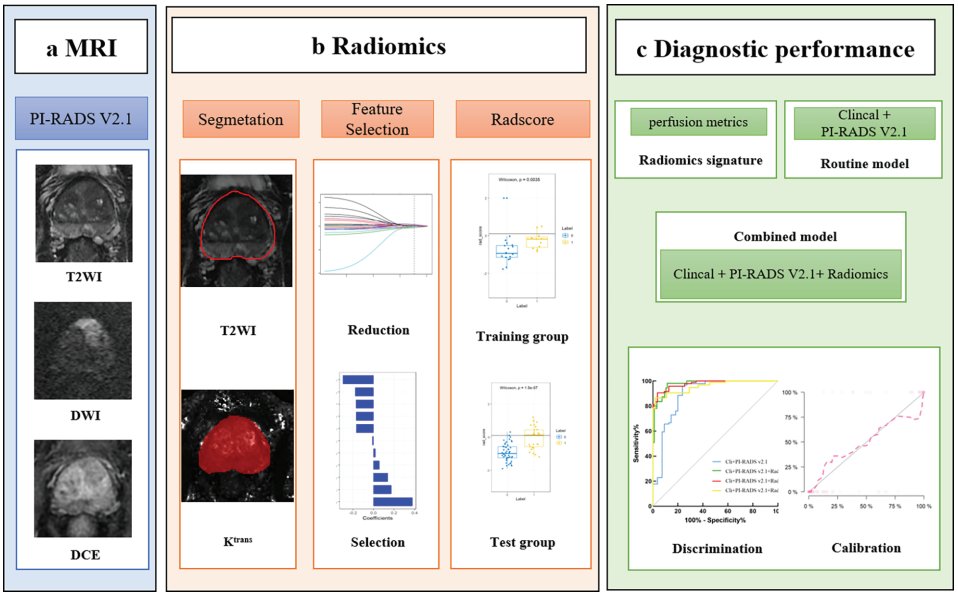

Figure 1. The study design and general process. DWI, Diffusion Weighted Imaging; T2WI, T2 Weighted Imaging; DCE, dynamic contrast-enhanced; MRI, magnetic resonance imaging; PI-RADS V2.1, prostate imaging reporting and data system version 2.1.

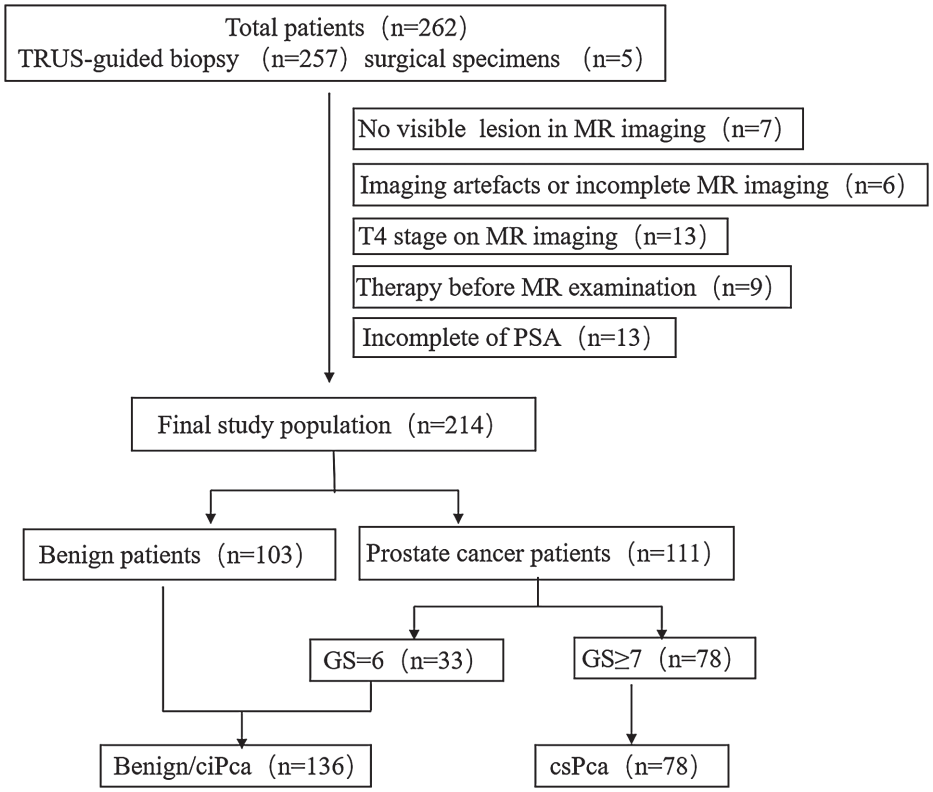

Figure 2. Flowchart of the patient screening process for the study. MR, magnetic resonance.

protocol comprised axial and coronal T2WI, DWI (including a dedicated b=1400 s/mm^2 sequence), and DCE (with an approximate time resolution of 10 seconds). Additional details on the specific imaging parameters are available in **Supplementary Table 1**.

Prostate imaging reporting and data system evaluation

Two experienced radiologists (CPW and JMT), each with over 5 years of experience in prostate MRI, independently reviewed the MR imaging. The assessment of prostate lesions

for each patient was conducted using prostate imaging reporting and data system version 2.1 (PI-RADS V2.1). The readers were blinded to pathological and PSA information. In case of disagreement, final prostate imaging reporting and data system (PI-RADS) scores were determined through discussion. The first reader (CPW) rescored all patients' MR imaging using PI-RADS V2.1 2 weeks after the initial assessment to evaluate intra-rater reliability.

Radiomics

Prostate separation

The DCE data of the prostate were processed using the ISP post-processing workstation (Philips Healthcare, Eindhoven, The Netherlands). An extended Tofts model was employed for the tracer-kinetic analysis of DCE-MR image, and the perfusion metrics (K^{trans}, V_e, K_{ep}) were subsequently analysed. Manual segmentation of the prostate was conducted utilising the ITK-SNAP software (open-source software, version 3.4.0, http://www.itksnap.org). YW, having over 8 years of experience in prostate MR imaging, delineated the volume of interest (VOI) along the boundaries of the prostate capsule, slice by slice, on MR imaging derived from perfusion parameter maps of 214 patients.

Feature extraction and radiomics signature establish

The radiomic features of the lesions, extracted using PyRadiomics (version 3.0, https://github.com/Radiomics/pyradiomics), an open-source Python package comprising a total of 960 features, extracted from the perfusion parameter map of each patient. The patients were randomly divided into two groups: 70% (n=151) for the training cohort to establish the predictive model and the remaining patients (n=63) for evaluating the predictive model. To standardise the value scales among radiomics features, individual feature values for all patients underwent normalisation using Z-scores ($(x–\mu)/\sigma$) before feature selection. Subsequently, a two-step feature selection approach was implemented, involving minimum-redundancy maximum-relevance (mRMR) and least absolute shrinkage and selection operator (LASSO). Initially, mRMR was employed to eliminate redundant and irrelevant features, retaining 20 essential features. Subsequently, LASSO was applied to meticulously choose an optimised subset from the retained features for constructing the final model. Tenfold cross-validation was employed to ascertain optimal values for λ. Ultimately, the most predictive features were selected based on their respective coefficients. The selection was based on computing a Radiomic signature (Rad-score) of each patient using a linear combination weighted by the selected feature coefficients within the predictive models.

Model building

Clinical-prostate imaging reporting and data system model

Univariate logistic regression analysis was conducted to evaluate potential clinical factors, including total PSA (tPSA), free PSA (fPSA), prostate volume, PSAD, and age. Subsequently, a Clinical-PI-RADS model was developed via multivariate logistic regression analysis, incorporating clinically significant characteristics and the PI-RADS score.

Clinical-prostate imaging reporting and data system-radiomics model

Clinical-PI-RADS-radiomics models were developed by combining the statistically significant features identified in univariate logistic regression analysis with PI-RADS score and the radiomics signature, employing multivariate logistic regression analysis to classify csPCa.

Statistical analyses

Measurement data distribution normality was assessed through the Kolmogorov-Smirnov test, and variance homogeneity was evaluated via Levene's test. Fisher's exact test or Chi-squared test was employed for assessing categorical variables when appropriate. T-test or Mann-Whitney U test was conducted on continuous variables based on their normality

Table 1. Clinical and magnetic resonance imaging characteristics of all 214 enrolled patients

Characteristic	Total (n=214)	csPCa (n=78)	non-csPCa (n=136)		*p*	Training cohort* (n=151)	Test cohort (n=63)		*p*
Age* (years)	68 (64, 74)	73 (66, 78)	67 (63, 72)	Z=–4.239	0.000	68 (64, 73)	70 (66, 76)	Z=–1.739	0.082
tPSA * (ng/mL^2)	13.51 (9.09, 26.49)	24.98 (11.30, 55.90)	11.04 (8.47, 18.03)	Z=–5.900	0.000	13.27 (8.62, 27.41)	15.08 (10.45, 26.27)	Z=–0.742	0.469
fPSA* (ng/mL^2)	1.74 (1.00, 3.08)	2.25 (1.20, 5, 34)	1.53 (0.96, 2.40)	Z=–3.423	0.001	1.73 (1.00, 3.08)	1.79 (1.07, 3.08)	Z=–0.480	0.631
PSAD* (ng/mL^2)	0.11 (0.08, 0.15)	0.50 (0.24, 1.05)	0.16 (0.10, 0.23)	Z=–8.240	0.000	0.20 (0.11, 0.39)	0.22 (0.13, 0.45)	Z=–0.857	0.391
Prostate volume* (mL)	66.83 (46.40, 100.25)	54.57 (37.91, 79.71)	78.90 (51.60, 105.50)	Z=–3.211	0.001	70.72 (47.36, 99.94)	63.86 (45.36, 103.26)	Z=–0.441	0.659
PI-RADS V2.1									
≤2	18	0	18	χ^2=69.747	0.000	13	5	χ^2=0.151	0.985
3	64	10	54			46	18		
4	74	22	52			52	22		
5	58	46	12			40	18		

tPSA, total prostate specific antigen; fPSA, free prostate specific antigen; PSAD, prostate specific antigen density; PI-RADS V2.1, prostate imaging reporting and data system version 2.1; csPCa, clinically significant prostate cancer; non-csPCa, non-clinically significant prostate cancer.

** Data are expressed as median (interquartile range).*

The Mann-Whitney U test was utilized for the comparative analysis of clinical databetween both group csPCa and group non-csPCa, as well as between the training cohortand the test cohort.

The Chi-squared test was utilized to compare the distribution of PI-RADS scores betweengroup csPCa and group non-csPCa, as well as between the training and test cohorts.

and homogeneity assumptions. The Weighted Kappa statistics test was utilised to assess inter-rater variability of the PI-RADS V2.1 score. The evaluation of the models' diagnostic performance in predicting csPCa involved calculating the area under curve (AUC), specificity (SP), sensitivity (SE), and accuracy (ACC). DeLong's test was employed to compare the AUCs between models. The calibration of the model was evaluated using the Hosmer-Lemeshow test. Statistical analyses were performed using R software (version 3.5.1, R Core Team, Oakland, CA, USA), SPSS (version 22.0, IBM, Armonk, NY, USA) and GraphPad Prism (version 8.3.1, GraphPad Software, La Jolla, CA, USA). Flowcharts were created by PowerPoint (version 2013, Microsoft, Seattle, WA, USA).

Results

Out of the initial 262 participants, 214 eligible patients were included, with 111 patients diagnosed with PCa and 103 with benign lesions. Among the patients diagnosed with PCa, 33 were classified as having non-clinically significant cancer based on their GS6 score. The patients were ultimately categorised into two groups: csPCa (n=78) and non-csPCa (n=136).

Clinical characteristics of patients

Baseline characteristics, including age, prostate volume, PI-RADS V2.1 score, tPSA, and fPSA, were presented in Table 1. Significant differences were observed ($p < 0.05$) between the csPCa group and the non-csPCa group regarding PV, tPSA, fPSA, PSAD, age, and PI-RADS V2.1 score. No statistically significant differences ($p > 0.05$) were observed in these characteristics between the training and test cohorts (Table 1).

Table 2. Clinical factors screening and clinical-prostate imaging reporting and data system model building for clinically significant prostate cancer prediction

	Univariate logistic analysis			Multivariate logistic analysis				
Clinical factors	Odds ratio (95% CI)	*p*	Clinical-PI-RADS model	*β*	Standard Error	Wald	Odds ratio (95% CI)	*p*
Age	1.106 (1.054, 1.161)	0.000	Age	0.064	0.034	3.599	1.066 (0.998, 1.138)	0.058
tPSA	1.065 (1.036, 1.094)	0.000	tPSA	0.050	0.027	3.481	1.051 (0.997, 1.107)	0.062
fPSA	1.128 (1.034, 1.230)	0.007	fPSA	–0.171	0.097	3.107	0.843 (0.697, 1.019)	0.078
PV	0.993 (0.983, 1.002)	0.113	PSAD	2.403	1.024	5.504	11.052 1 (0.485, 82.258)	0.019
PSAD	33.372 (8.649, 128.762)	0.000	PI-RADS V2.1	0.965	0.316	9.332	2.625 (1.413, 4.876)	0.002

CI, confidence interval; PI-RADS V2.1, prostate imaging reporting and data system version 2.1; PV, prostate volume.

Inter-observer and intra-observer agreement

The inter-reader agreement for PI-RADS scores between the two readers (CPW and JMT) was moderate (κ=0.603; 95% confidence interval [95% CI] (0.521, 0.685), *Z*=13.683, *p*=0.000). The intra-observer agreement (the first time and the second time) of the reader (CPW) was good (κ=0.857; 95% CI (0.790, 0.924), *Z*=8.432, *p*=0.000).

Radiomic signature

Through feature selection, the number of features was reduced to 17, 18 and 11 for K^{trans}, V_e, and K_{ep}, respectively. These selected features were then incorporated into the radiomic signature known as Rad-score. The relative weight of these features, along with the Rad-score, can be observed in **Supplementary Table 2** and **Supplementary Figure 1**. The Rad-score reflects the probability of csPCa. To assess any differences between the csPCa group and non-csPCa group in both training and test cohorts, the *Wilcoxon* test was employed (**Supplementary Figure 2**).

Development and performance of the predictive model

Five clinical features, namely age, tPSA, fPSA, PV, and PSAD, underwent univariate regression analysis for screening. PSAD, age, tPSA, and fPSA were identified as independent clinical predictors for csPCa (Table 2). Then, combining the aforementioned four independent clinical factors with the PI-RADS score to construct the Clinical-PI-RADS model to predict csPCa by multivariate logistic analysis, PSAD, and PI-RADS were considered independent influencing factors of the Clinical-PI-RADS model (Table 2). Additionally, combining the Rad-score with clinical factors and PI-RADS score resulted in the development of three Clinical-PI-RADS-Rad score combined models for K^{trans}, V_e, and K_{ep} parameters, respectively. Age, PSAD, PI-RADS, and Rad-score are considered independent influencing factors for the Clinical-PI-RADS-Rad score combined model (Tables 3–5).

The diagnostic efficiency of the radiomic signature, Clinical-PI-RADS model, and Clinical-PI-RADS-Rad score models are outlined in Table 6. The ROC of predictive models for csPCa plots are displayed in Figure 3. Results of the DeLong test between models for csPCa are displayed in Figure 4.

The models exhibited a satisfactory fit (as determined by the Hosmer-Lemeshow Goodness-of-Fit test; $p > 0.05$) in both the training and test cohorts. The calibration curves of combined models are displayed in **Supplementary Figure 3**.

Table 3. Clinical-prostate imaging reporting and data system-rad score (K^{trans}) model building for clinically significant prostate cancer prediction

Clinical-PI-RADS-Radscore (K^{trans}) model	*β*	Standard Error	Wald	Odds ratio (95% CI)	*p*
Age	0.106	0.052	4.183	1.112 (1.004, 1.232)	0.041
tPSA	0.054	0.040	1.834	1.056 (0.976, 1.141)	0.176
fPSA	–0.184	0.124	2.184	0.832 (0.652, 1.062)	0.139
PSAD	3.011	1.418	4.506	20.298 (1.260, 327.054)	0.034
PI-RADS V2.1	1.148	0.457	6.314	3.153 (1.287, 7.721)	0.012
Radscore-K^{trans}	2.227	0.472	22.238	9.268 (3.674, 23.384)	0.000

Table 4. Clinical-prostate imaging reporting and data system-radscore (V_e) model building for clinically significant prostate cancer prediction

Clinical-PI-RADS-Radscore (v_e) model	*β*	Standard Error	Wald	odds ratio (95% CI)	*p*
Age	0.101	0.047	4.604	1.107 (1.009, 1.214)	0.032
tPSA	0.066	0.044	2.224	1.069 (0.979, 1.166)	0.136
fPSA	–0.267	0.161	2.728	0.766 (0.558, 1.051)	0.099
PSAD	2.531	1.447	3.059	12.568 (0.737, 214.313)	0.040
PI-RADS V2.1	1.194	0.442	7.290	3.300 (1.387, 7.851)	0.007
Radscore-V_e	1.326	0.281	22.267	3.766 (2.171, 6.533)	0.000

Table 5. Clinical-prostate imaging reporting and data system-radscore (K_{ep}) model building for clinically significant prostate cancer prediction

Clinical-PI-RADS-Radscore (K_{ep}) model	*β*	Standard Error	Wald	Odds ratio (95% CI)	*p*
Age	0.097	0.045	4.677	1.102 (1.009, 1.202)	0.031
tPSA	0.062	0.038	2.619	1.064 (0.987, 1.147)	0.106
fPSA	–0.158	0.116	1.863	0.854 (0.681, 1.071)	0.172
PSAD	1.958	1.694	1.335	7.028 (3.256, 196.100)	0.047
PI-RADS V2.1	0.922	0.436	4.472	2.515 (1.196, 5.290)	0.015
Radscore-K_{ep}	1.768	0.380	21.683	5.859 (2.782, 12.342)	0.000

Discussions

In this retrospective study, diagnostic models were constructed based on PI-RADS scores and clinical data, with or without radiomics extracted from perfusion parameters of DCE imaging. The combined model, incorporating radiomics of perfusion parameters based on the region of interest (ROI) of the whole prostate gland, improved the accuracy of predicting csPCa compared to the conventional diagnostic model.

Table 6. Diagnostic performance of the models for predicting clinically significant prostate cancer

	Training cohort						Test cohort					
	AUC (CI)	SE	SP	PPV	NPV	ACC	AUC (CI)	SE	SP	PPV	NPV	ACC
Radiomics (K^{trans})	0.86 (0.80, 0.92)	0.78	0.78	0.86	0.67	0.78	0.86 (0.76, 0.95)	0.78	0.83	0.89	0.68	0.79
Radiomics (V_e)	0.88 (0.83, 0.93)	0.82	0.82	0.89	0.73	0.82	0.87 (0.78, 0.95)	0.78	0.87	0.91	0.69	0.81
Radiomics (K_{ep})	0.87 (0.81, 0.93)	0.82	0.82	0.89	0.73	0.81	0.86 (0.76, 0.96)	0.78	0.87	0.92	0.69	0.83
Clinical + PI-RADS V2.1	0.89 (0.84, 0.95)	0.93	0.87	0.75	0.97	0.89	0.91 (0.84, 0.98)	0.85	0.86	0.74	0.93	0.86
Clinical + PI-RADS V2.1 + Radiomics (K^{trans})	0.97 (0.95, 0.99)	0.82	0.94	0.91	0.89	0.89	0.97 (0.94, 1.00)	0.88	0.97	0.96	0.93	0.94
Clinical + PI-RADS V2.1 + Radiomics (V_e)	0.98 (0.96, 1.00)	0.98	0.93	0.87	0.99	0.95	0.95 (0.91, 1.00)	0.83	0.92	0.87	0.90	0.89
Clinical + PI-RADS V2.1+Radiomics (K_{ep})	0.96 (0.93, 0.98)	0.74	0.99	0.98	0.80	0.87	0.97 (0.94, 1.00)	0.88	0.95	0.91	0.93	0.92

AUC, area under curve; CI, confidence interval; SE, sensitivity; SP, specificity; PPV, positive predictive value; NPV, negative predictive value; ACC, accuracy.

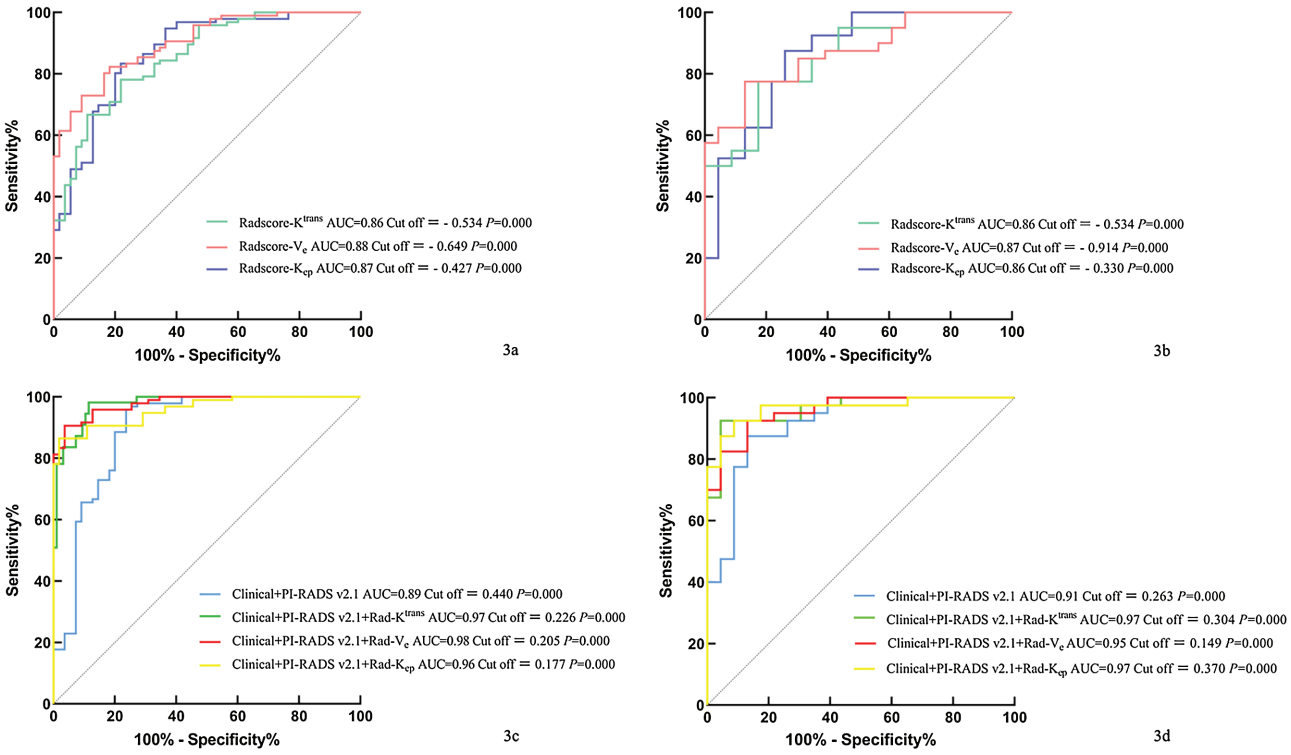

Figure 3. Receiver operating characteristic curves in the differentiation of clinically significant prostate cancer from no-clinically significant prostate cancer by radiomics signature in training cohort (3a), test cohort (3b) and models in training cohort (3c), test cohort (3d).

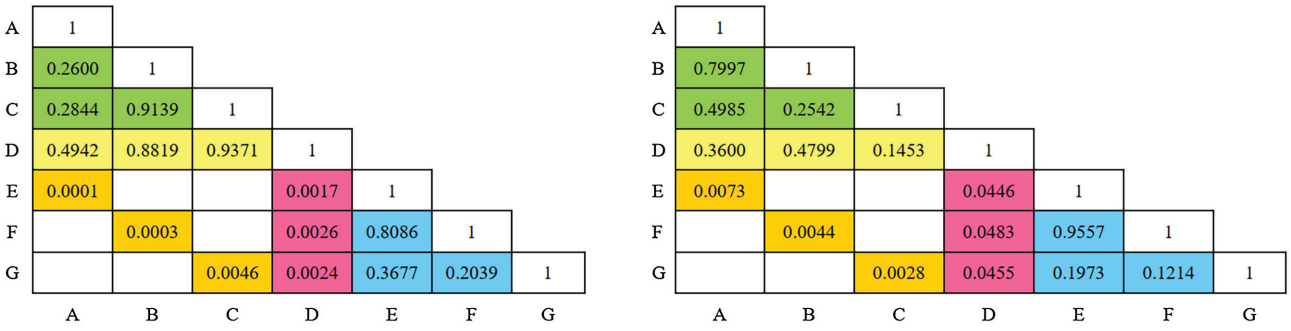

Figure 4. The *p* value of *the* DeLong test between predictive models in the training cohort (left) and in the test cohort (right). A: Radscore-K^{trans}; B: Radscore-V_e; C: Radscore-K_{ep}; D: Clinical + PI-RADS V2.1; E: combined model-K^{trans}; F: combined model-V_e; G: combined model-K_{ep}. Colour representation: red: combined models compare with Clinical + PI-RADS V2.1 model; orange: comparison of radiomics signature and combined model for K^{trans}, V_e, and K_{ep}, respectively; green: comparison between radiomics signatures; blue: comparison between combined models; yellow: radiomics signatures compare with Clinical + PI-RADS V2.1 model.

The quantitative modelling approach in pharmacokinetics directly computes the local concentration of contrast agents within the tissue. It estimates pharmacokinetic parameters believed to reflect pathophysiological changes in the microenvironment of PCa (Tofts et al, 1999). Our study analysed three of the most common quantitative parameters used in studies about DCE including K^{trans}, V_e and K_{ep}. In PCa, many studies have demonstrated elevated levels of K^{trans}, K_{ep}, and V_e compared to normal tissue (Padhani et al, 2000; Kozlowski et al, 2006; Ocak et al, 2007). The increase in PCa enhancement after gadolinium-based contrast agent administration is influenced by several variables, such as the quantity and permeability of blood vessels, which are believed to be higher in tumours than in healthy prostatic tissue in the peripheral zone. Dynamic contrast-enhanced MR imaging of the prostate leverages this distinction to discern features of the tumour's local microcirculatory environment (Verma et al, 2012). The density of microvessels is correlated with tumour stage, recurrent metastatic potential, and prognosis in patients with PCa (Tan et al, 2015). Rosenkrantz et al (2013) discovered that sensitivity for peripheral zone tumours increased when employing either a semiquantitative or quantitative DCE approach, as opposed to qualitative analysis. Our findings are consistent with the above study and demonstrate that radiomics-based quantitative perfusion parameters have high diagnostic efficacy in predicting csPCa. However, a meta-analysis conducted by Zeng et al (2021) revealed that DCE imaging limits utility for ill-defined lesions and suggested the need for more appropriate methods to improve csPCa detection. Histologic factors can affect image contrast in MR imaging of PCa (Vos et al, 2008). However, increased cellular density and nucleomegaly may also indicate inflammation, prostatic intraepithelial neoplasia, or changes in lumen size due to cystically dilated glands, fibrosis, or areas of atrophy. These benign abnormalities are linked to false-positive MR imaging findings or limited radiologic-pathologic volumetric correlation. The overlapping perfusion parameter values between csPCa and non-csPCa may result from the histological diagnosis of most of these normal regions as benign prostatic hyperplasia. Increased capillary permeability, vascularity, and interstitial hypertension are considered underlying mechanisms contributing to the visual overlap between tumours and these normal tissues (Sureka et al, 2019). We performed an analysis on the whole gland, which contained both information on the tumour and its surroundings. Meanwhile, to the subjectivity of the margin of tumour in the prostate, gland segmentation is easier to achieve than the segmentation of the tumour zone.

The findings of our study demonstrate that radiomics based on DCE perfusion parameters exhibit potential in predicting csPCa, with no statistically significant difference in diagnostic efficacy compared to the conventional model (based on clinical features and PI-RADS V2.1). Radiomics has proven effective in predicting csPCa, achieving favourable diagnostic efficiency. Li et al (2020) suggest that radiomics-based machine-learning models can enhance the prediction accuracy of clinically significant cancers. By incorporating perfusion data from high spatiotemporal resolution DCE MRI protocols as input features, machine learning classifiers are able to better differentiate moderate-to-severe PCa when combined

with non-contrast sequences, compared to using non-contrast sequences alone. The risk stratification capability for machine learning classifiers, particularly in distinguishing between moderate and high-risk PCa in the peripheral region, is significantly enhanced when utilising perfusion information extracted from high spatiotemporal resolution DCE MRI acquisition schemes compared to classifiers relying solely on T2WI/DWI information (Winkel et al, 2020). As demonstrated by Antonelli et al (2019), zone-specific models that combine prostate specific antigen density and radiomic features surpassed assessments made by experienced radiologists in detecting csPCa. Also showing promising results in detecting csPCa in the peripheral zone, approaches that extract radiomic features from prostate mpMRI using a VOI achieved the highest AUC of 0.87 with the XGBoost classifier (Bleker et al, 2019).

Our study employs radiomics to uncover crucial insights aimed at enhancing diagnostic efficiency in the detection of csPCa. It illustrates that the use of radiomics with perfusion parameters yields strong diagnostic performance for predicting csPCa. Furthermore, the amalgamated model, which integrates radiomics with conventional parameters, demonstrates superior diagnostic capability compared to relying solely on perfusion-based radiomics or conventional models. Our research findings align with those of Feng et al (2024), whose study suggests that the predictive efficacy of the bpMRI model for csPCa was marginally inferior to that of the mpMRI model but superior to that of the PI-RADS score. This emphasises the significance of incorporating DCE derived parameters into conventional models to enhance their ability to differentiate between csPCa and non-csPCa.

Our study has certain limitations. Firstly, the sample size was moderate and could benefit from an increased cohort of patients. Secondly, future studies should incorporate an external validation cohort to evaluate the reproducibility of our established method. Finally, our retrospective design introduces the possibility of selection bias; however, we contend that this potential bias is minimal, given the consecutive sampling method employed.

Conclusion

Incorporating radiomic information extracted from DCE perfusion parameters into the diagnostic model can improve the accuracy of detecting csPCa compared to the conventional model based solely on clinical and PI-RADS scores. This may lead to the avoidance of unnecessary biopsies and a more precise treatment plan for patients. Further research, such as prospective randomised trials and the integration of other artificial intelligence-based techniques, is necessary to better select patients and indications before recommending the general use of bpMRI in the clinical setting.

Key points

- Dynamic enhancement perfusion parameters based on radiomics show satisfactory performance in predicting csPCa.
- There were no significant differences in predicting csPCa among the MR dynamic enhanced quantitative perfusion parameters K^{trans}, K_{ep}, and V_e.
- The combination model incorporating radiomics extracted from perfusion parameters, clinical data, and PI-RADS V2.1 score can enhance the predictive capability for csPCa compared to using the radiomic signature or conventional model alone.

Author details

[1]Department of Radiology, The Central Hospital of Wuhan, Tongji Medical College, Huazhong University of Science and Technology, Wuhan, Hubei, China

[2]Department of Radiology, Guiyang Guanshanhu Maternal and Child Health Hospital, Guiyang, Guizhou, China

[3]Department of Radiology, Ping An Healthcare Diagnostics Center, Wuhan, Hubei, China

Availability of data and materials

All the data of this study are included in this article.

Author contributions

YW and CPW conceived and drafted the manuscript. FM and JMT contributed to the collection of MR imaging and clinical data. JMT and CPW were responsible for interpreting the MR imaging. YW was responsible for delineating the region of interest in the MR imaging. CPW and YW performed the software operation and statistical analysis. All authors contributed to important editorial changes in the manuscript. All authors read and approved the final manuscript. All authors have participated sufficiently in the work and agreed to be accountable for all aspects of the work.

Ethics approval and consent to participate

This retrospective study received approval from the Institutional Review Boards of the Central Hospital of Wuhan (Ethics number: WHZXKYL2024-042). The study protocol complied with the Declaration of Helsinki, and informed consent was obtained from all participants.

Acknowledgement

We gratefully thank Dr. Fei Xiong for the operation of the R software help.

Funding

This research received no external funding.

Conflict of interest

Chipeng Wang was an employee of Ping An Healthcare Diagnostics Center. Other authors declare no conflict of interest.

Supplementary material

Supplementary material associated with this article can be found, in the online version, at https://www.magonlinelibrary.com/doi/suppl/10.12968/hmed.2024.0131.

References

Ahmed HU, Akin O, Coleman JA et al. Transatlantic consensus group on active surveillance and focal therapy for prostate cancer. BJU Int. 2012;109(11):1636–1647. https://doi.org/10.1111/j.1464-410X.2011.10633.x

Antonelli M, Johnston EW, Dikaios N et al. Machine learning classifiers can predict Gleason pattern 4 prostate cancer with greater accuracy than experienced radiologists. Eur Radiol. 2019;29(9):4754–4764. https://doi.org/10.1007/s00330-019-06244-2

Bass EJ, Pantovic A, Connor M et al. A systematic review and meta-analysis of the diagnostic accuracy of biparametric prostate MRI for prostate cancer in men at risk. Prostate Cancer Prostatic Dis. 2020;24(3):596–611. https://doi.org/10.1038/s41391-020-00298-w

Belue MJ, Yilmaz EC, Daryanani A, Turkbey B. Current status of biparametric MRI in prostate cancer diagnosis: literature analysis. Life. 2022;12(6):804. https://doi.org/10.3390/life12060804

Bleker J, Kwee TC, Dierckx RAJO et al. Multiparametric MRI and auto-fixed volume of interest-based radiomics signature for clinically significant peripheral zone prostate cancer. Eur Radiol. 2019;30(3):1313–1324. https://doi.org/10.1007/s00330-019-06488-y

Boesen L, Nørgaard N, Løgager V et al. Assessment of the diagnostic accuracy of biparametric magnetic resonance imaging for prostate cancer in biopsy-naive men. JAMA Netw Open. 2018;1(2):e180219. https://doi.org/10.1001/jamanetworkopen.2018.0219

Bosaily AE, Frangou E, Ahmed HU et al. Additional value of dynamic contrast-enhanced sequences in multiparametric prostate magnetic resonance imaging: data from the PROMIS study. Eur Urol. 2020;78(4):503–511. https://doi.org/10.1016/j.eururo.2020.03.002

Cindil E, Oner Y, Sendur HN et al. The utility of diffusion-weighted imaging and perfusion magnetic resonance imaging parameters for detecting clinically significant prostate cancer. Can Assoc Radiol J. 2019;70(4):441–451. https://doi.org/10.1016/j.carj.2019.07.005

Feng X, Chen X, Peng P et al. Values of multiparametric and biparametric MRI in diagnosing clinically significant prostate cancer: a multivariate analysis. BMC Urol. 2024;24(1):40. https://doi.org/10.1186/s12894-024-01411-0

Kozlowski P, Chang S, Jones E et al. Combined diffusion-weighted and dynamic contrast-enhanced MRI for prostate cancer diagnosis—correlation with biopsy and histopathology. J Magn Reson Imaging. 2006;24(1):108–113. https://doi.org/10.1002/jmri.20626

Kuhl CK, Bruhn R, Kramer N et al. Abbreviated biparametric prostate MR imaging in men with elevated prostate-specific antigen. Radiology. 2017;285(2):493–505. https://doi.org/10.1148/radiol.2017170129

Li M, Chen T, Zhao W et al. Radiomics prediction model for the improved diagnosis of clinically significant prostate cancer on biparametric MRI. Quant Imaging Med Surg. 2020;10(2):368–379. https://doi.org/10.21037/qims.2019.12.06

Ocak I, Bernardo M, Metzger G et al. Dynamic contrast-enhanced MRI of prostate cancer at 3 T: a study of pharmacokinetic parameters. AJR Am J Roentgenol. 2007;189(4):W192–W201. https://doi.org/10.2214/AJR.06.1329

Padhani AR, Gapinski CJ, Macvicar DA et al. Dynamic contrast enhanced MRI of prostate cancer: correlation with morphology and tumour stage, histological grade and PSA. Clin Radiol. 2000;55(2):99–109. https://doi.org/10.1053/crad.1999.0327

Rosenkrantz AB, Sabach A, Babb JS et al. Prostate cancer: comparison of dynamic contrast-enhanced MRI techniques for localization of peripheral zone tumor. AJR Am J Roentgenol. 2013;201(3):W471–W478. https://doi.org/10.2214/AJR.12.9737

Siegel RL, Miller KD, Jemal A. Cancer statistics. CA Cancer J Clin. 2015;65(1):5–29. https://doi.org/10.3322/caac.21254

Stavrinides V, Giganti F, Trock B et al. Five-year outcomes of magnetic resonance imaging-based active surveillance for prostate cancer: a large cohort study. Eur Urol. 2020;78(3):443–451. https://doi.org/10.1016/j.eururo.2020.03.035

Sureka B, Elhence P, Khera PS et al. Quantitative contrast-enhanced perfusion kinetics in multiparametric MRI in differentiating prostate cancer from chronic prostatitis: results from a pilot study. Br J Radiol. 2019;92(1100):20190181. https://doi.org/10.1259/bjr.20190181

Tan CH, Hobbs BP, Wei W, Kundra V. Dynamic contrast-enhanced MRI for the detection of prostate cancer: meta-analysis. Am J Roentgenol. 2015;204(4):W439–W448. https://doi.org/10.2214/AJR.14.13373

Tavakoli AA, Hielscher T, Badura P et al. Contribution of dynamic contrast-enhanced and diffusion MRI to PI-RADS for detecting clinically significant prostate cancer. Radiology. 2023;306(1):186–199. https://doi.org/10.1148/radiol.212692

Tofts PS, Brix G, Buckley DL et al. Estimating kinetic parameters from dynamic contrast-enhanced T(1)-weighted MRI of a diffusable tracer: standardized quantities and symbols. J Magn Reson Imaging. 1999;10(3):223–232. https://doi.org/10.1002/(SICI)1522-2586(199909)10:3<223::AID-JMRI2>3.0.CO;2-S

Verma S, Turkbey B, Muradyan N et al. Overview of dynamic contrast-enhanced MRI in prostate cancer diagnosis and management. AJR Am J Roentgenol. 2012;198(6):1277–1288. https://doi.org/10.2214/AJR.12.8510

Vos PC, Hambrock T, Hulsbergen-van de Kaa CA et al. Computerized analysis of prostate lesions in the peripheral zone using dynamic contrast enhanced MRI. Med Phys. 2008;35(3):888–899. https://doi.org/10.1118/1.2836419

Wei C, Jin B, Szewczyk-Bieda M et al. Quantitative parameters in dynamic contrast-enhanced magnetic resonance imaging for the detection and characterization of prostate cancer. Oncotarget. 2018;9(22):15997–16007. https://doi.org/10.18632/oncotarget.24652

Winkel DJ, Breit HC, Block TK, Boll DT, Heye TJ. High spatiotemporal resolution dynamic contrast-enhanced MRI improves the image-based discrimination of histopathology risk groups of peripheral zone prostate cancer: a supervised machine learning approach. Eur Radiol. 2020;30(9):4828–4837. https://doi.org/10.1007/s00330-020-06849-y

Zeng J, Cheng Q, Zhang D et al. Diagnostic ability of dynamic contrast-enhanced magnetic resonance imaging for prostate cancer and clinically significant prostate cancer in equivocal lesions: a systematic review and meta-analysis. Front Oncol. 2021;11:620628. https://doi.org/10.3389/fonc.2021.620628

Zhao J, Kader A, Mangarova DB et al. Dynamic contrast-enhanced MRI of prostate lesions of simultaneous [(68)Ga]Ga-PSMA-11 PET/MRI: comparison between intraprostatic lesions and correlation between perfusion parameters. Cancers (Basel). 2021;13(6):1404. https://doi.org/10.3390/cancers13061404